Designing and Characterizing Hyperpolarizable Silicon Nanoparticles for Magnetic Resonance Imaging
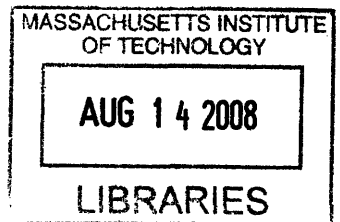
by

Melis Nuray Anahtar

SUBMITTED TO THE DEPARTMENT OF MECHANICAL ENGINEERING IN
PARTIAL FULFILLMENT OF THE REQUIREMENTS FOR THE DEGREE OF

BACHELOR OF SCIENCE IN ENGINEERING
AT THE
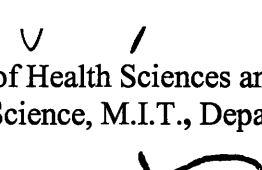MASSACHUSETTS INSTITUTE OF TECHNOLOGY

JUNE 2008

Signature of Author:_
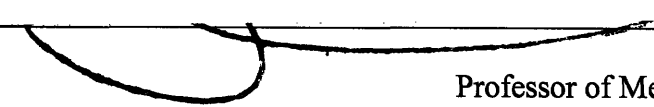
Department of Mechanical Engineering
May 9, 2008

Certified by:_

Sangeeta N. Bhatia
Professor of Health Sciences and Technology/ Electrical Engineering & Computer
Science, M.I.T., Department of Medicine, Brigham & Women's Hospital
Thesis Supervisor

Accepted by:_

John H. Lienhard V
Professor of Mechanical Engineering
Chairman, Undergraduate Thesis Committee

(Page Intentionally Left Blank)

Designing and Characterizing Hyperpolarizable Silicon Nanoparticles for Magnetic Resonance Imaging

by

Melis Nuray Anahtar

Submitted to the Department of Mechanical Engineering
on May 9, 2008 in partial fulfillment of the
requirements for the Degree of Bachelor of Science in Engineering
as recommended by the Department of Mechanical Engineering

ABSTRACT

Magnetic Resonance Imaging (MRI) is one of the most powerful noninvasive tools for diagnosing human disease, but its utility is limited because current contrast agents are ineffective when imaging air-tissue interfaces, in regions with low signal-to-noise ratios, or in areas that undergo motion, like the heart and bowel. A technique called dynamic nuclear polarization can be used to hyperpolarize nuclei and achieve dramatic MRI signal enhancement with minimal background noise. It has been shown that ball-milled silicon nanoparticles have the advantageous properties of hyperpolarizability and biodegradability, but *in vivo* utilization requires the modification of the particle surface to prevent aggregation that leads to very fast removal from circulation through phagocytosis by the liver, spleen, and lymph nodes. This thesis describes a method to functionalize hyperpolarizable silicon nanoparticles using silane chemistry and coating by poly(ethylene glycol). The particles were characterized using dynamic light scattering, scanning electron microscopy, and laser Doppler electrophoresis. The extent of amination was quantified using a fluorescamine assay, and stability was assessed by visualizing flocculation and measuring aggregation in different solvents. The functionalized particles were stable in solutions that resemble physiological conditions. These silicon nanoparticles can potentially be used for *in vivo* cancer imaging to enable early diagnoses and assist with clinical decision-making through disease monitoring.

Thesis Supervisor: Sangeeta N. Bhatia
Title: Professor of Health Sciences and Technology/ Electrical Engineering & Computer Science, M.I.T., Department of Medicine, Brigham & Women's Hospital

(Page Intentionally Left Blank)

Acknowledgments

I would like to thank several people who have helped me tremendously with completing this thesis. First and foremost, I am very grateful to Professor Sangeeta Bhatia for her constant support throughout the year and for the privilege of working in the Laboratory for Multiscale Regenerative Technology. It has been a wonderful to learn so much about nanotechnology and tissue engineering, while enjoying the company of all the fun and inspiring people in the lab, including the many talented undergraduates. In particular, I would like to thank Yin Ren for his guidance, assistance with getting the project off the ground, and for proofreading this thesis, Geoff von Maltzahn for his patience and willingness to answer my never-ending list of questions, and Amit Agrawal for his advice and discussions.

Additionally, I would like to thank several collaborators at Harvard University–Professor Charles Marcus, Jacob Aptekar, Alison Lynn Hill, Fettah Kosar, and Chinh Vo–whose expertise in physics and material science made this project possible. Also, thanks to Ji Ho Park at the University of California San Diego for sharing his knowledge of silicon nanoparticles.

Finally, I must thank my family and friends, including my Mom, Dad, Melodi, and Shaye, for their endless words of encouragement.

(Page Intentionally Left Blank)

Table of Contents

(Page Intentionally Left Blank)

1 Introduction

Nanoparticle-based contrast agents have the potential to revolutionize Magnetic Resonance Imaging (MRI) and cancer detection. The most commonly used MRI contrast agents are gadolinium chelates, which provide positive contrast through an enhancement in T_1-weighting. An alternative to gadolinium-based agents is superparamagnetic iron oxide nanoparticles (SPIO), which have an iron oxide core surrounded by a layer of bio-compatible polymers. SPIO can be multifunctional [1] and indicate physiological and molecular changes in addition to anatomical changes [2]. The shortcoming of SPIO is that they provide negative contrast on T_2-weighed images, which makes them less sensitive than T_1-type agents [3]. SPIO cannot be used effectively when imaging at air-tissue interfaces, in regions with low signal-to-noise ratios, or in areas that undergo motion, like the heart and bowel. A new contrast agent is needed for imaging certain regions of the body, including the lungs, bowel, liver, pancreas, and lymph nodes. Silicon nanoparticles are a promising solution because they can be detected with MRI after hyperpolarization [4] and are thought to be biodegradable [5].

The focus of this thesis was to functionalize silicon nanoparticles for the targeted imaging of tumors by hyperpolarization. This was done by determining the key properties of silicon nanoparticles including size and charge, modifying their surface characteristics by attaching biocompatible polymers, and evaluating their stability in solution.

2 Background

2.1 MRI

Medical MRI uses a strong magnetic field to align the magnetic moment of nuclei that have an odd number of nucleons like ^{1}H, ^{13}C, and ^{31}P. Then, a radio frequency pulse that targets a single type of atom is administered, and one out of every few million atoms are induced to change their spin from the low energy state to the high energy state [6]. When the pulse is over, the atoms relax back to their natural spin state while releasing energy, which can be detected by the MRI machine and converted into a picture. By simply changing the frequency of the pulse, doctors can specifically examine different parts of the body, like bones, tumors, organs, and blood.

MRI is already one of the most powerful noninvasive tools for diagnosing human disease, but its utility is limited because it distinguishes healthy from abnormal tissue using nonspecific macroscopic physical differences, like inherent energy and density. This nonspecific imaging technique makes it extremely hard to discriminate a tumor from a fluid-filled cavity by simply examining an MR image. To overcome this obstacle, certain anatomical structures are routinely visualized by injecting the patient with a contrast agent, such as Gadolinium, Iron, and Magnesium [7]. Gadolinium in particular is very commonly used–millions of doses are administered annually–but some patients have been found to develop adverse reactions like nephrogenic systemic fibrosis [8].

2.2 Nanoparticle-based contrast agents

Superparamagnetic iron oxide nanoparticles (SPIO) can be used for MRI imaging because of the effects of the large dipolar magnetic field gradient that they create on neighboring protons. SPIOs consist of a magnetite (Fe_3O_4) core and a hydrophilic coating, such as dextran or siloxanes[2]. Their surfaces can be modified to allow cell-specific binding and they have been studied extensively for drug delivery, diagnostics, and cell-tracking applications. Depending on their application, SPIO range from tens of nanometers to over several microns, when the cores contain multiple iron oxide crystals (Figure 1).
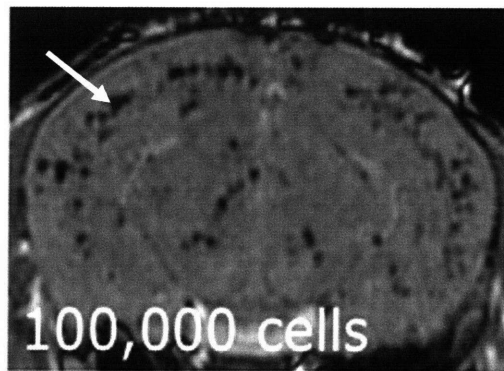

Figure 1: MR detection of cells labeled with micron-sized iron oxide particles in the brain of a mouse. The arrow indicates signal voids from the presence of IO particles [21].

Cells labeled with as little as 1.4 picograms of SPIO can be detected using a 4.7T MRI scanner [9]. Their sensitivity has enabled them to be used for many applications, like tracking stem cells in the brain [10] and labeling immune T cells [11], which provides insight into biological processes like stem-cell differentiation and cell-trafficking [12]. In addition to the reasons above, SPIO are gaining popularity because several compounds have been FDA approved and are commercially available, like Bayer Pharmaceutical's Feridex IV®.

However, the main limitation of iron oxide nanoparticles is that they are negative contrast agents and are consequently imaged indirectly by the absence of signal (Figure 1) [13]. When the MRI scanner imposes an external magnetic field, the SPIO magnetic

dipoles align and change the local magnetic field, which causes nearby rotating protons to dephase. It is this proton dephasing that is detected by a T2-weighted MR image, not the SPIO themselves [2]. Thus, SPIO are difficult to detect in regions with low native signal-to-noise ratio, cannot be used to image areas that move, like the heart, and are difficult to use for reliably tracking cells *in vivo*. Given these limitations, it is beneficial to examine other nanoparticle-based contrast agents.

2.3 General hyperpolarization MRI

Normal MRI is limited by the fact that the magnetic energy of nuclear spins is low compared to the thermal energy at room temperature [4]. Researchers currently work around this limitation by imaging with very powerful magnetic fields of 9 Teslas and above, which can increase the polarization of ^{1}H from 5 ppm to 70 ppm [4]. These magnets are large, expensive, and potentially dangerous. There is still much room for improvement, especially when imaging nuclei with lower magnetic moments, like ^{13}C and ^{15}N.

A novel technique for achieving dramatic MRI signal enhancement with minimal background noise is called hyperpolarization. Hyperpolarization can be achieved in several ways including dynamic nuclear polarization (DNP), which transfers polarization from unpaired electrons to nuclei using microwave irradiation. There are three well-studied methods of DNP: the Overhauser effect, the solid effect, and the thermal mixing effect. The DNP set-up that will be used to hyperpolarize the silicon crystals characterized in this thesis will primarily utilize the thermal mixing effect. Thermal mixing is the most efficient existing irradiation mechanism, and basically involves the transfer of energy from electron spin packets to nuclear spins [14]. The main components

of the apparatus are the cryostat fitted with a 6 T superconducting magnet, a Gunn diode to supply the microwaves, and a coil to measure NMR signal.

DNP has been used extensively on ^{3}He, ^{129}Xe, and ^{13}C. The drawback to these particular contrast agents is that they can only be detected for a very short time after hyperpolarization due to their very short relaxation periods. The *in vivo* T_1 relaxation time is 7–9 minutes for ^{3}He [15], 14.1±1.6 seconds for ^{129}Xe [16], and 20±2 seconds for ^{13}C [17]. Thus, their applications are limited to observing phenomena that occur on comparable timescales, like imaging the lungs with inhalable ^{3}He and ^{129}Xe gas, and tracing metabolites with ^{13}C [18]. Figure 2 shows the potential for using hyperpolarized ^{13}C for *in vivo* imaging of the kidneys and heart.

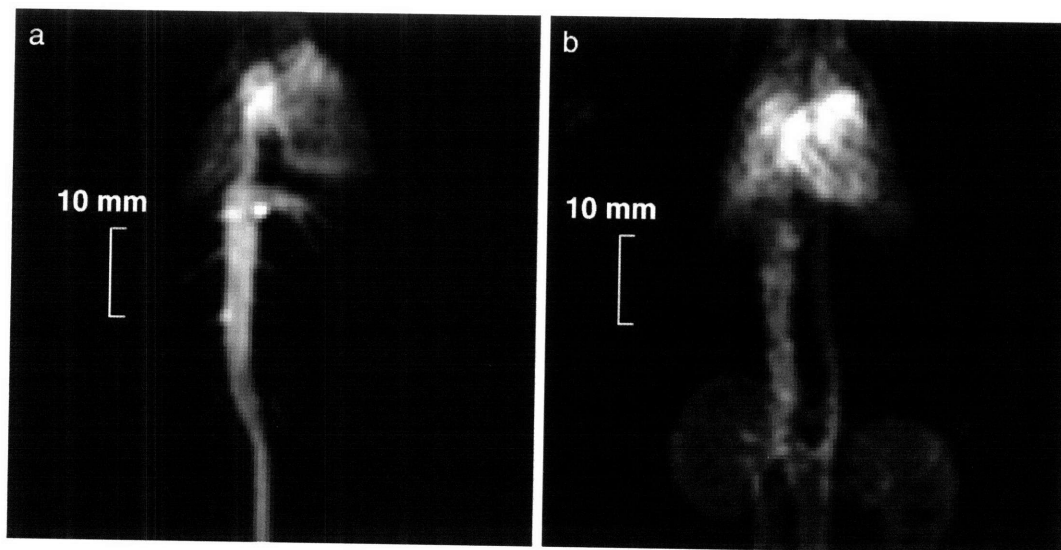**Figure 2:** *In vivo* angiographic images before (a) and after (b) injecting ^{13}C hyperpolarized urea into a rat [17].

2.4 Hyperpolarization of silicon for contrast imaging

Unlike the noble gases or ^{13}C currently used for hyperpolarization and MR imaging, silicon has been shown to have very long relaxation times–up to five hours [19]–and can consequently can be injected into the bloodstream and tracked throughout

the body. Multi-hour relaxation times enable particle imaging after allowing sufficient time for tumor localization [20] and enabling long-term cell tracking for the elucidation of disease mechanisms [21].

The solid state of Si provides a useful platform for a wide variety of functionalization strategies, and applications for drug delivery. Moreover, silicon is known to be non-toxic [22] and it is metabolized and secreted by the body [5, 23]. In addition to long detection times, the MRI signal-to-noise ratio from these ^{29}Si particles can be theoretically be boosted by several orders of magnitude [4] through DNP. These properties–long relaxation times, DNP signal enhancement, and ease of functionalization compared to nobel gases–make hyperpolarized silicon nanoparticles a very appealing MRI contrast agent.

The silicon nanoparticles must meet specific requirements for hyperpolarization and functionalization. This study uses particles ground from P-type, <1-1-1>, Boron-doped silicon wafers with a resistivity of 30–100 kΩ-cm, diameter of 4", and thickness of 1016 μm. Crystalline silicon has a face-centered diamond cubic
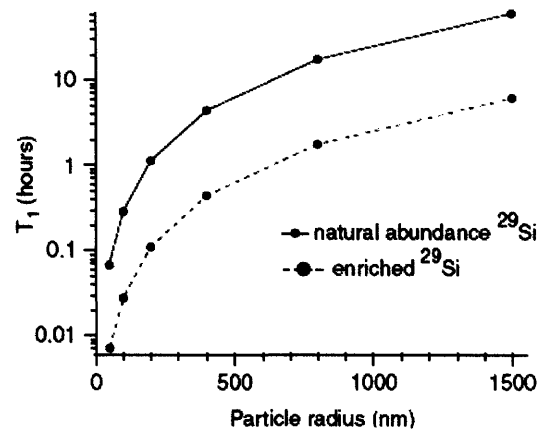
Figure 3: Simulation of relaxation time as a function of silicon particle radius [24].

crystal structure, with nuclei that can be polarized by nuclear spin diffusion. These same wafers are used in the semiconductor industry and contain an initial, intrinsic defect density of 1–5×10^{11} defects/cm^3. This indicates that ball-milled particles less than a micron should not have any electron defects. However, electron spin resonance (ESR)

14

data indicates a significant number of defects from "dangling bonds," or broken covalent bonds, in these particles, which affects their hyperpolarizability and relaxation times. Simulations have recently shown that the relaxation time is also a function of the silicon particle size, where large particles have longer T_1 relaxation times, as shown in Figure 3 [24]. Since silicon can be hyperpolarized, detected by MRI, modified using well-characterized surface chemistry, and biodegraded, it is a very promising nanoparticle material.

2.5 Imaging and therapeutic applications

Cancer is the leading cause of death for adults in the United States due to many factors including the inherent complexity of the disease, inadequate detection methods leading to late diagnoses, and the lack of specificity of anticancer agents [25]. But the early identification of tumors can significantly improve clinical outcomes, especially for colorectal and lung cancers which have usually metastasized by the time of diagnosis [26].

Nanoparticles have tremendous applications for cancer detection and treatment because they can be designed to home to tumors [1], be detected by MRI and fluorescence [25], deliver chemotherapeutics [27], track cells (Section 1.2.1), and destroy tumors by localized heating [28]. Tumor localization can occurs mainly through the enhanced permeability and retention (EPR) phenomenon, which exploits the natural "leakiness" of tumor vessels that enables cancer cells to access the nutrients that they need to proliferate [29]. Through EPR, nanoparticles injected into the bloodstream passively accumulate more in tumors than the bloodstream and healthy organs [30]. Active targeting, where particles are attached to nucleic acids or protein fragments that

enable them to specifically recognize and bind to receptors residing on cancer cells, could theoretically be used for molecular recognition and enhanced drug delivery to poorly vascularized regions [1]. Such tumor-homing peptides have been identified, such as the peptide sequence of Arginine-Glycine-Aspartate (RGD) that binds to the surface of angiogenic blood vessels [31, 32].

Once the nanoparticles home to the tumor, they can be imaged *in vivo* using different modes of detection depending on the nanoparticle material. For example, SPIO are detected using MRI, quantum dots with fluorescence, and bismuth sulfide nanoparticles with computed tomography (CT) imaging. In addition to being imaged, some particles can even be designed to directly deliver therapeutic payloads [33].

2.6 Silicon nanoparticle design criteria

The nanoparticles' size and shape are important design criteria [34, 35]. The ball milling process can be used to make particles of varying sizes–from less than 100 nm to greater than a micron. The grinding conditions must be optimized to ensure that the particles are the proper size for *in vivo* tumor imaging applications. The particles must be large enough to have long relaxation times in order to be detected with MRI. But, if the particles are to circulate in the bloodstream, extravasate near the tumor, and accumulate in the tumor interstitium at high enough concentrations to be imaged, then they must have long *in vivo* circulation times by avoiding capture by the reticuloendothelial system (RES).

It is difficult to quantify the minimum circulation time needed for the detection of a tumor using hyperpolarized silicon, but therapeutic drugs take at least six hours in circulation for EPR to take effect [20]. If the nanoparticle can be detected with high

sensitivity, as is theoretically the case with hyperpolarized particles, then the circulation time could be much shorter. The minimum circulation time necessary for tumor localization and visualization by EPR affects the nanoparticle diameter. For example, if the particles must be detected after thirty minutes or more then they must have a radius greater than 100 nm.

In addition to affecting relaxation times, size is a very important determinant for how long the particles can circulate in the bloodstream before being extracted by the reticuloendothelial system, which is comprised of the spleen, liver, and bone marrow. The spleen is a major obstacle for nanoparticles because it is essentially a biological sieve. It contains two types of tissue, one with macrophage immune cells that recognize and degrade encapsulated foreign bodies in the bloodstream, and another that filters out worn-out red blood cells and other rigid and abnormally-shaped objects. The width of the interendothelial slits in the spleen is between 200 nm–1 μm [36]. Minor blockages of these slits are tolerable, but spherical particles over a micron in diameter are likely to get trapped in the spleen and consequently have very short circulation times of a few minutes [37]. The liver has a slightly lower blood perfusion rate than the spleen. The liver endothelial cells contain fenestrations with a mean diameter of 175 nm that redirect nanoparticles from the bloodstream into the lymphatic drainage; nanoparticles with two dimensions greater than 300 nm are likely to bypass the fenestrated epithelium [37]. In addition to the fenestrations, the liver also contains macrophages that actively remove nanoparticles from the bloodstream. The nanoparticle surface must be modified to avoid recognition by macrophages; this can be achieved through coating with polymers or by mimicking the red blood cells' oligosaccharide coating, since they are able to stay in

circulation for 110–120 days [36]. Finally, the lung and kidneys are not part of the reticuloendothelial system but they have the highest blood perfusion rates of any organ. Their vasculature can be easily passed by particles between from 15 nm–7 μm [37] In summary, long-circulating particles would ideally be designed with one or two dimensions between 200 nm and a micron in order to bypass filtration by the major organs of the body.

When nanoparticle-mediated tumor imaging relies on passive targeting through EPR, the particles must be able to permeate the tumor microcirculation. The tumor pore cut-off size is highly variable and depends on both the microenvironment of the tumor and the tumor type. Pore cut-off sizes can vary from 7–2,000 nm [38]. Other barriers to the transport of molecules into tumors are the high tumor interstitial pressures that have a tendency to push everything out, and the abnormal architecture that makes extravasation slow [39].

Nanoparticle surface characteristics can affect uptake as well. Neutral particles are phagocytosed at a slower rate than highly cationic or anionic particles. They are also less toxic to immune cells and less likely to bind to plasma proteins [40, 53]. Poly(ethylene glycol) (PEG) is a non-toxic and non-immunogenic polymer that is used to coat nanoparticles and proteins to increase the compounds' circulation time and water solubility, while reducing toxicity and renal clearance. In aqueous solutions, each ethylene glycol unit in PEG associates with a water molecule and the nanoparticle becomes encapsulated in a protective hydration sphere. This prevents proteins from adsorbing to the nanoparticle surface, which would otherwise make the particle a clear

target for phagocytosis by the reticuloendothelial system [41]. For these reasons, PEG polymers are conjugated to the silicon nanoparticles in this study.

2.7 General procedure for functionalization

One of the most common methods of functionalizing oxidized metals is through a reaction with a silane, which has a general formula of $X_3Si(CH_2)_nY$. For silica particles grown by the Stöber process, coating is often performed with an alkoxysilane like tetraethoxysilane (TEOS) in solution [42]. The surface properties of silanated particles can cause them to aggregate, but coating the particles with PEG polymers reduces inter-particle interactions and improves biocompatibility [43]. The general schematic of nanoparticle functionalization used in this paper is outlined in Figure 4; the silane has an amine functional group that reacts with an NHS-group on the PEG chain to form a covalent bond.
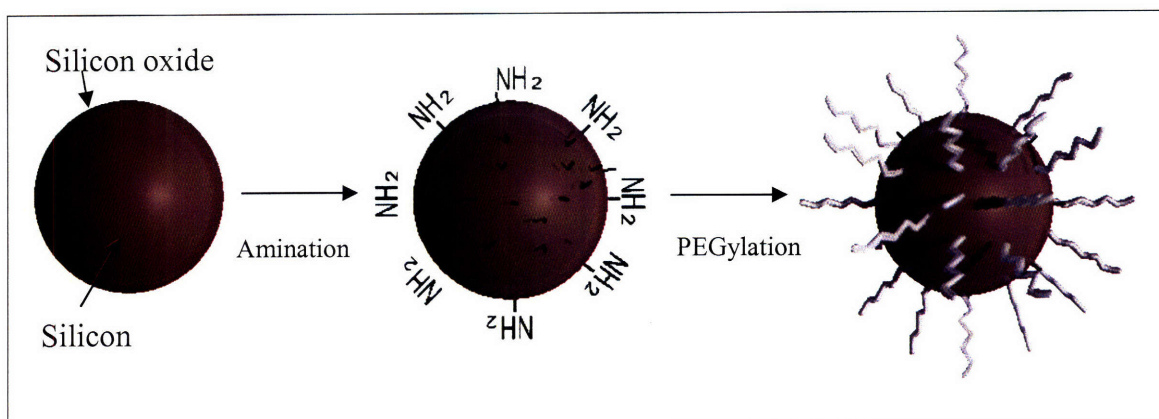

Figure 4: Schematic of silicon nanoparticle functionalization.

19

3 Experimental Procedures

3.1 Particle preparation

Silicon nanoparticles were prepared by grinding a silicon wafer (4" Sq1, Silicon Quest International and Silicon DSP) in a ball mill (400 rpm, Retsch PM 100). The grinding proceeded in three stages: a ten-minute dry grind using 1 cm diameter balls, followed by a four-hour grind in 20 mL of ethanol, and ending with a sixteen-hour grind using 3 mm diameter balls.

After grinding, the nanoparticle surface was cleaned by hydrofluoric acid (HF) etching, which selectively removes the silicon dioxide film that naturally grows on silicon surfaces exposed to air. HF is poisonous and must be handled with extreme caution. The particles were immersed in an HF solution for 10-30 minutes. The HF was removed through six washes; each time, the particles were spun at 12,000×g for five minutes, the supernatant was replaced with 100% ethanol, and the solution was sonicated (1 minute, 20% amplitude, Branson Digital Sonifier.)

The mean particle size, size distribution, and polydispersity were determined using dynamic light scattering (DLS, Nano ZS90, Malvern) at room temperature in water. A typical size distribution is illustrated in Figure 5. In this example, the particles in the first peak comprise 33.3% of the volume of the sample, with a mean diameter of 328 nm and width (polydispersity index) of 124 nm. The second peak was filtered out in subsequent steps, but consisted of particles above 5 μm. Scanning electron microscopy was also used to visualize the particle size distribution and shape.
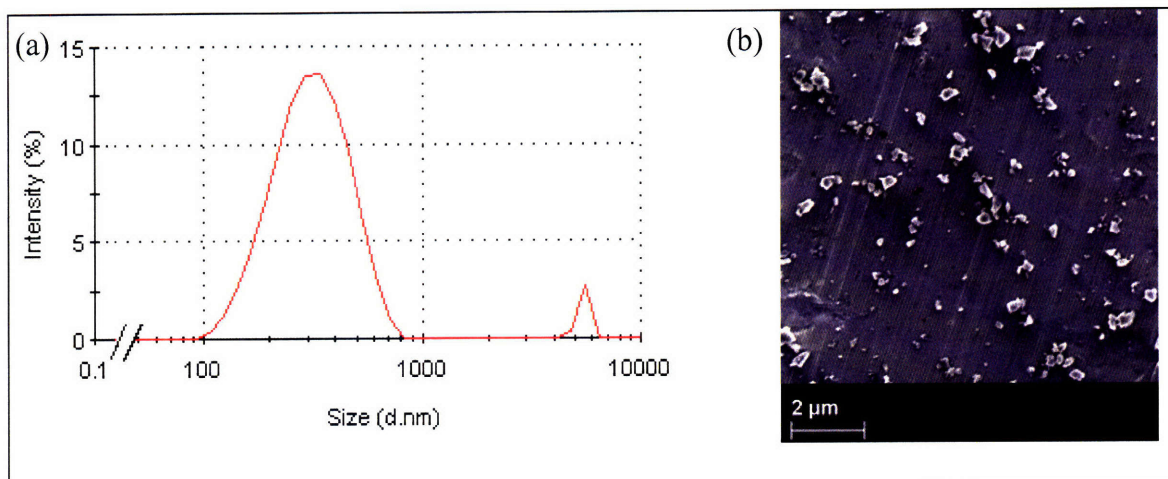
Figure 5: Size distribution (a) determined by the relative intensity of light scattered by particles and (b) imaged with a scanning electron microscope.

3.2 Amination

Amination was performed using either (3-Aminopropyl)triethoxysilane (APTES, Sigma, 99%) alone or as a 1:2 mixture by volume of APTES with bis-(triethoxysilyl)ethane (BTEOSE, Aldrich, 96%) or (3-trihydroxysilyl)propyl methylphosphonate (THPMP, Aldrich, 42 wt% in H_2O). Approximately 100 mg of silicon nanoparticles were added to 45 mL of acidified 70% ethanol (0.04% v/v, adjusted to pH 3.5) or methanol buffer (0.1 mM $NaHCO_3$ in methanol) and the solution was placed in an ultrasonic bath (Bransonic, 2210) for five minutes. To the nanoparticle solution, 0.10–0.15 M of silane was added and the solution was shaken for 18–24 hours. In some cases, the solution was then heated in a 65°C water bath for two hours. Excess silanes were removed from the nanoparticle solution by washing and resuspending three times in methanol buffer, with the final resuspension performed with 10 mL of ethanol or methanol buffer.

Amination was assessed using fluorescamine and ninhydrin colorimetric assays. The fluorescamine assay detects only primary aliphatic amines, while the ninhydrin assay

detects both primary and secondary amines. Before performing the assays, the concentrations of all of the particles were equalized by adjusting their absorption at 420 nm to 1.50 ± 0.05 (for 40 µL of sample in a clear 96-well plate). The fluoresamine reagent was prepared by dissolving 3.5 mg of fluorescamine (Sigma) in 1 mL of dimethyl sulfoxide (DMSO). Within a 96-well standard opaque tray, 10 µL of the fluorescamine solution were added simultaneously to each well containing 40 µL of nanoparticles and mixed thoroughly for one minute. Fluorescence was measured using an excitation at 390 nm and emission at 465 nm (SpectraMax Gemini XPS, Molecular Devices).

To perform the ninhydrin assay, ninhydrin solution (2% in DMSO and pH 5.2 acetate buffer, Sigma) was mixed with samples in a 2:1 ratio (20 µL sample: 10 µL ninhydrin), boiled for 10 minutes, cooled to room temperature, and diluted three-fold with ethanol. The absorbance was read at $\lambda_{max}= 570$ nm.

Additionally, the particle surface charge was measured using laser Doppler electrophoresis (Nano ZS90, Malvern) by adding 25-100 µL of nanoparticle solution to 1 mL of water or 0.1 M 2-(N-morpholino)ethanesulfonic acid buffer (MES, pH 6).

3.3 PEGylation

Aminated particles were coated with polyethylene glycol (PEG) polymers to confer stability and biocompatibility. Three types of polymers were used. The first has a terminal methoxy cap at one end and an amine-reactive succimidyl α-methylbutanoate (mPEG-SMB, Nektar) at the other, and a total molecular weight of 10,000 g/mol or 20,000 g/mol. The second is capped with an amine-reactive N-Hydroxysuccinimide and a maleimide, which couples to thiol groups (NHS-PEG-MAL, Nektar, 5000 g/mol). The third polymer served as a negative control because it was capped by a methoxy group and

an amine group (mPEG-Amine, Nektar, 20000 g/mol), neither of which reacts with amines on the nanoparticle surface.

In the PEGylation reaction, 10 mg PEG was mixed in 500 μL of methanol buffer and heated briefly at 50°C to dissolve. Approximately 0.1 mg of aminated particles (100 μL in solution) were added to this solution and it was placed in an ultrasonic bath for 1–3 hours. To remove the unreacted PEG, samples were centrifuged (13,000×g for 10 minutes) and resuspended twice in methanol and finally in a phosphate-buffered saline buffer solution (PBS, 0.1 M Na_2PO_4, 0.015 M NaCl buffer).

3.4 Stability

Stability was assessed by visualizing flocculation and measuring particle size and aggregation using dynamic light scattering. Previous studies have demonstrated that bare silica and aminated particles flocculate in 5% NaCl aqueous solutions [43], PBS, and 10% fetal bovine serum (FBS). If particles remained homogenous when added to 1 mL of these solutions, or could easily be redispersed by gentle flicking, they were considered to be stable and successfully PEGylated.

3.5 Cytotoxicity

The toxicity of unmodified silicon nanoparticles was assessed using a Calcein AM Viability Assay. Calcein AM is a membrane permeable nonfluorescent molecule that is taken-up by cells via incubation and hydrolyzed by endogenous esterases into green fluorescent calcein. It is used to quantify the number of live cells, since healthy cells retain and process calcein after uptake but dead cells do not [44].

HeLA cells were placed in a 96-well tissue culture plate and incubated for 24 hours. Bare nanoparticles suspended in 10% FBS were added in triplicates with serial dilutions from a stock solution of 1 mg/ml, and caffeine was used as a control. The cells were incubated with the particles at 37° C with gentle rocking, and after three hours 100 µL of 2 µM Calcein AM in PBS was added to each well. After 30 minutes of incubation at 37° C, the fluorescence was measured on a fluorescence plate reader with the excitation wavelength at 485 nm and the emission wavelength of 530 nm.

4 Results and Discussion

The goal of this experiment was to functionalize silicon nanoparticles using silane chemistry and PEG polymers, and then demonstrate their stability. Functionalization is a critical prerequisite for the *in vivo* utilization of these nanoparticles.

4.1 Optimal amination conditions

Ball-milled silicon particles were successfully aminated using organofunctional silanes. The optimal amination conditions were determined by varying the pH of the solution, solvent composition, temperature of reaction, and type of organosilane. Amination was most successful when the nanoparticles were HF-etched and suspended in a 70% ethanol solution adjusted to a pH of about 3.
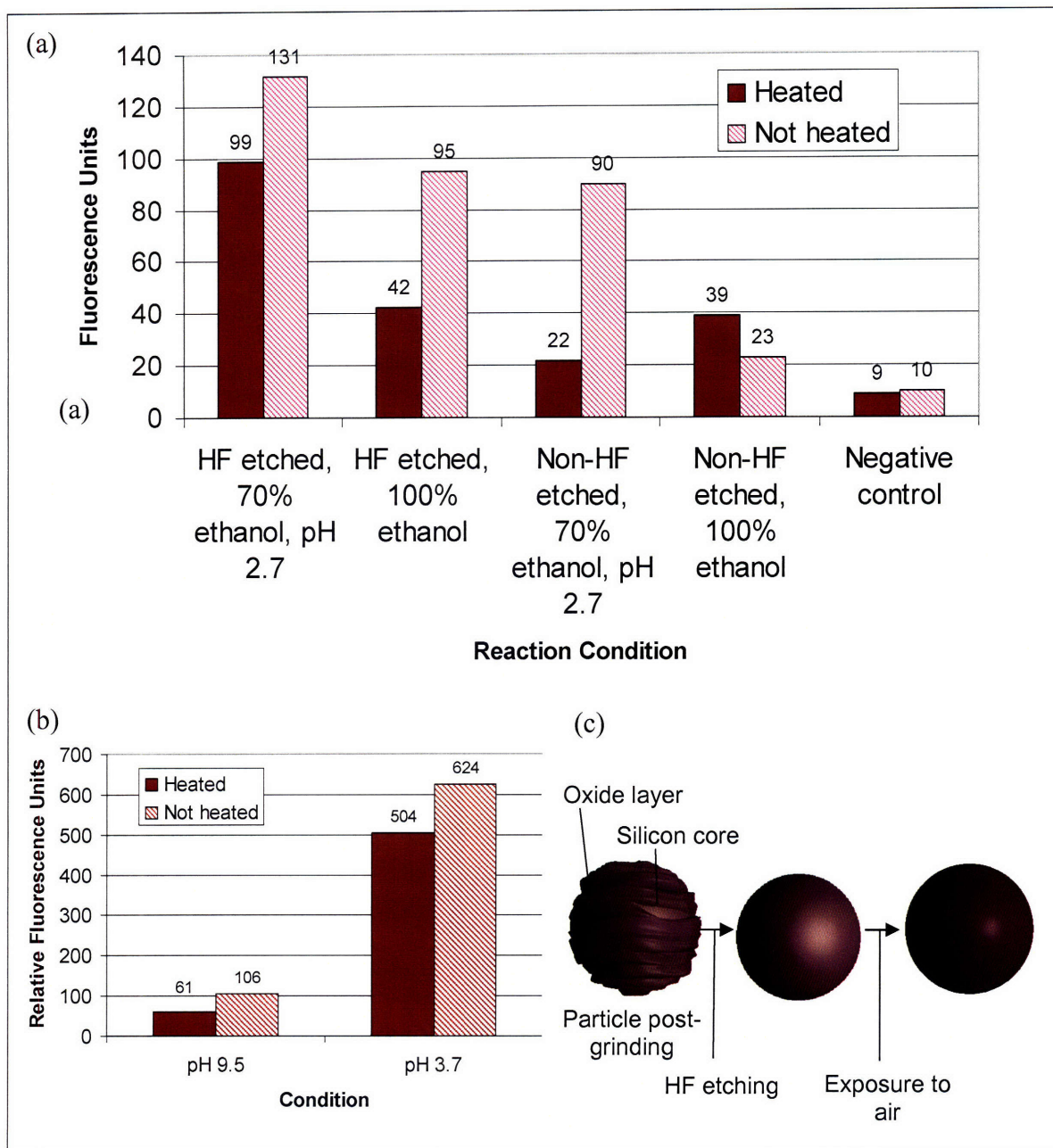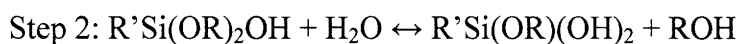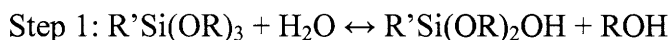
Figure 6: Effect of solvent (a), pH (b), and HF etching (a and b) on amination with APTES and BTEOSE, as measured by a fluorescamine assay. Schematic of the effect of HF etching (c).

There are several explanations for this finding. Several reactions occur when APTES is added to a nanoparticle solution; first hydrolysis, then competition between grafting onto the silicon dioxide surface and homocondensation [45].

Hydrolysis occurs in a stepwise manner when the three ethoxysilyl groups of APTES come into contact with water [46] (for APTES: R = ethoxy group, R' = aminopropyl group):

Step 1: $R'Si(OR)_3 + H_2O \leftrightarrow R'Si(OR)_2OH + ROH$

Step 2: $R'Si(OR)_2OH + H_2O \leftrightarrow R'Si(OR)(OH)_2 + ROH$

Step 3: $R'Si(OR)(OH)_2 + H_2O \leftrightarrow R'Si(OH)_3 + ROH$

The removal of the first ethoxy group is the rate-determining step of hydrolysis and occurs with first-order kinetics with respect to the silane [46]. Since the Si-OH moiety is very reactive, the trihydroxsilyl group that results from hydrolysis is much more likely to react with the surface of the nanoparticle. This modification of APTES occurs in the presence of water and may explain why amination is more successful in a 70% ethanol solution than pure ethanol.

In addition to hydrolyzing, the APTES monomers can react either with the silicon nanoparticle surface or with other APTES monomers, in a process called homocondensation. It has been shown that performing the amination reaction under pH conditions less than 4.5 minimizes homocondensation and thus promotes grafting onto the oxide surface [47]. Figures 6a and 6b illustrate that decreasing the pH from 9.5 to 3.7 promotes a five-fold increase in amination. Another explanation for the advantage of a low pH environment is that it prevents "upside-down" silane absorption, where the inverted silane's amino terminus electrostatically interacts with the metal oxide [48].

Despite the safety hazards, HF etching was used in order to maintain some control over the oxide layer thickness. The schematic of HF etching is shown in Figure 6c, in which the hydrofluoric acid selectively removes the silicon oxide layer that grows

26

naturally on the silicon particle surface. More uniform oxide layers may lead to better contact with APTES, since Figure 6 demonstrates the slight increase in amination that resulted after etching. Additionally, the particles were aminated within a few hours of HF etching and sonicated for the same amount of time, ensuring that the oxide layer thickness was comparable between experiments and particle batches.

Previous studies have demonstrated that amination reaction kinetics are influenced by temperature; for example, smooth APTES films were grown on silicon wafers by maintaining solution temperatures at 75° C [49]. However, Figures 6a and 6b demonstrate that higher reaction temperatures do not promote amination for these particles. This difference may be attributed to differences in the silicon form. Thin APTES layers may be easier to form on flat, motionless silicon wafers, than on small particles being shaken in solution.

Initially, amination was measured using both fluorescamine and ninhydrin assays. There was consistent disagreement between the two tests; the ninhydrin assay was not sensitive enough to detect the amines on the particles treated with both APTES and APTES with THPMP, but it showed above-background amination for the particles with APTES and BTEOSE. This would indicate that the APTES and BTEOSE treated particles contained secondary amines that only the ninhydrin assay was able to detect. However, an additional control with particles treated with BTEOSE alone showed a similarly elevated absorbance level, though there should not have been any amines in the sample. It is possible that the BTEOSE stock was contaminated with a compound containing amines like bis-aminosilane. Given the results of the control, the fluorescamine assay was used as the primary amine detection method.

In addition to chemical assays, the accumulation of amines could be indirectly monitored by measuring the particles' surface charge and observing the solution's colloidal state. The surface of the unmodified silicon nanoparticles is composed of hydroxyl groups from the oxidized silicon. Particles treated with APTES should have surfaces coated with propylamines, which have a K_b of $4.7 \cdot 10^{-4}$ M and become protonated and positively charged in acidic solutions (Figure 7a) [42]. The actual surface charge can be measured by the zeta potential, since particles become ionized and associate with charged species within an aqueous medium. The zeta potentials were measured in water and MES buffer, and the results strongly correlate with the hypothesized charges (see Figure 8). Unmodified particles have a very negative surface charge of -17.0 ± 7.2 mV (see Figure 7a). Particles aminated with only APTES have a positive charge of 12.6 ± 6.0 mV. Particles treated with APTES and THPMP are slightly less charged than those with only APTES and have a larger standard deviation. This is consistent with previous studies because THPMP contains a phosphonate group that is negatively charged at physiological pH 7.4 [42]. An unexpected finding was that particles treated with APTES and BTEOSE have a very high positive charge of 34.5 ± 6.3 mV.
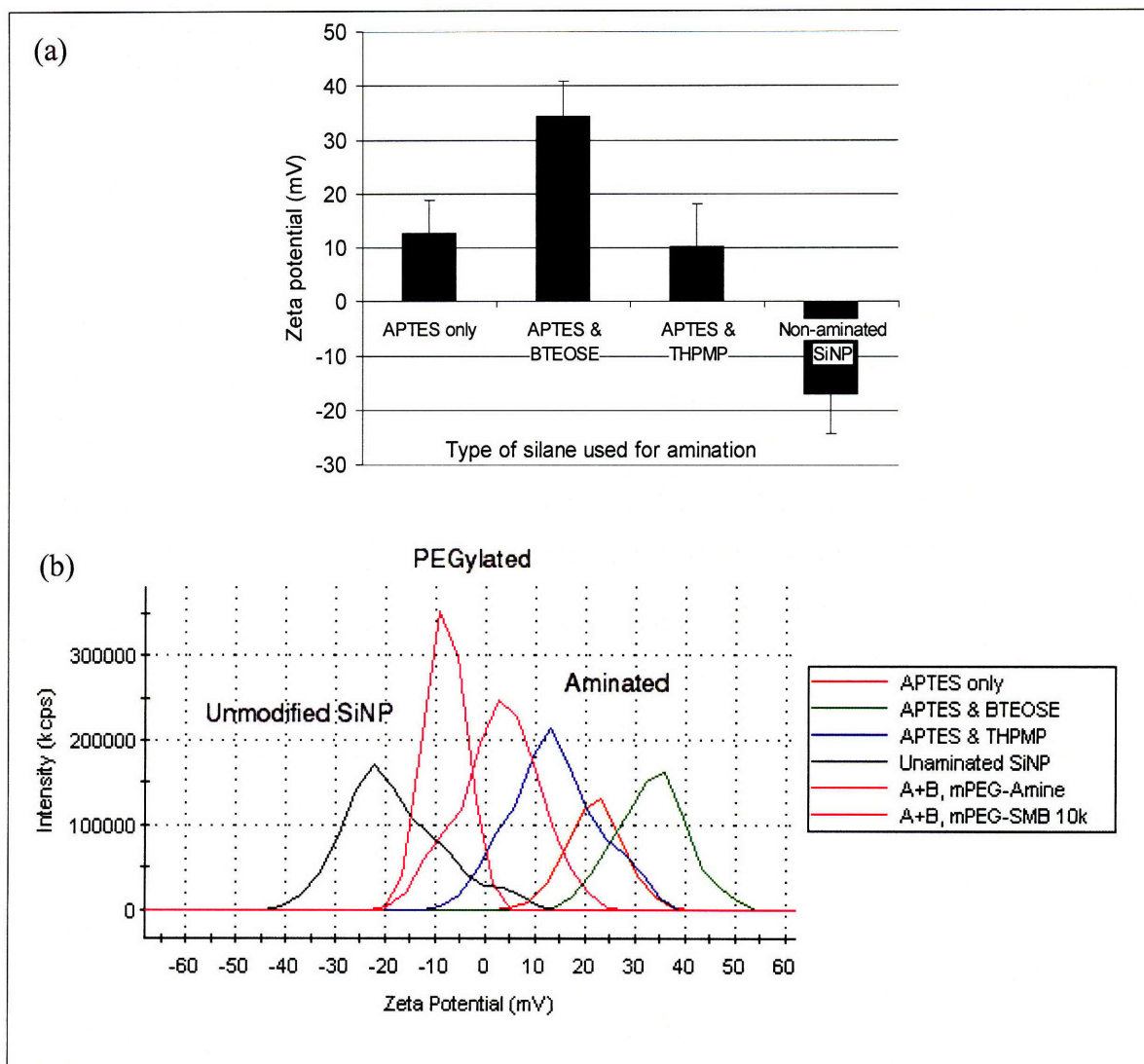
Figure 7: Zeta potential distribution (measured in water) of (a) particles treated with different silanes and (b) particles that were aminated and then PEGylated.
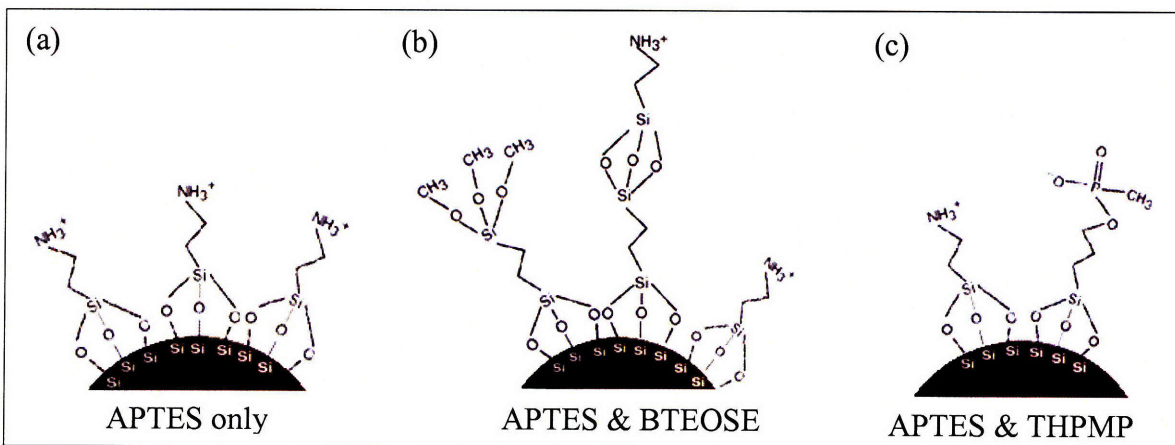

Figure 8: Schematic of silicon oxide surface aminated with (a) APTES only, (b) APTES & BTEOSE, and (c) APTES & THPMP.

29

The high charge of the APTES and BTEOSE surface could be due the same contaminant in BTEOSE that caused the false-positive in the ninhydrin assay, or because the BTEOSE linker absorbed to the silicon surface and evenly distributing the APTES. It has been shown that the BTEOSE layer is porous and intermixed with APTES [48]. Thus, the BTEOSE may be preventing horizontal polymerization between two surface-bound APTES monomers, or eliminating back-bonding of the positively charged amine on APTES with the negatively charged silicon hydroxide surface. Both of these scenarios would reduce the number of free primary amines on the surface. The lower concentration of APTES may also be causing the growth of a thinner and more uniform APTES film.

4.2 Evidence of PEGylation via stability of particles

The utilization of silicon nanoparticles *in vivo* requires them to be stable in a variety of media. If the nanoparticles flocculate in solution to form micron-sized aggregates, they are much more likely to be removed from the bloodstream, thereby decreasing their circulation time and tumor imaging abilities. But achieving colloidal stability is not trivial; previous studies have demonstrated that bare and aminated particles aggregate immediately when exposed to 0.15 M salt solutions, which are comparable to physiological conditions [50]. One method of simultaneously preventing aggregation and improving biocompatibility is by coating the nanoparticles with poly(ethylene glycol) (PEG) polymers.

Figure 9: (Top) mPEG-SMB and (bottom) MAL-NHS-PEG
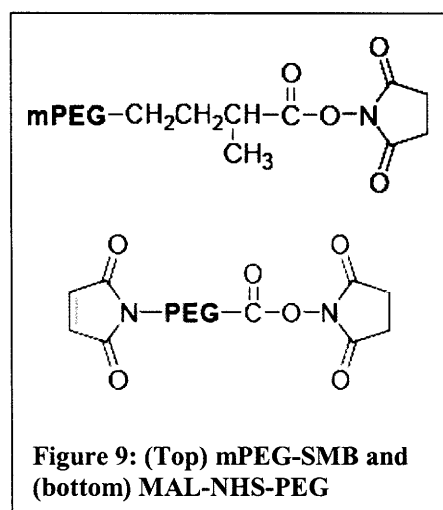
The aminated particles in this experiment were PEGylated with either mPEG-SMB or NHS-PEG-MAL (Figure 9). Both SMB and NHS are reactive with amines on the particle surface. As a negative control, mPEG-Amine polymer was used because it does not contain amine-reactive groups and therefore should not conjugate to the nanoparticle surface.

The stability of nanoparticles in solution was assessed using both dynamic light scattering (DLS) and visual determination of flocculation and sedimentation. These criteria are valid because particles in liquid media move primarily through thermal motion and sedimentation because of gravity. Microscopic thermal motion is equivalent to Brownian motion, which is measured by the DLS instrument to determine particle size. Sedimentation can also be observed by placing the nanoparticle sample in different media and observing the sedimentation rate.

The DLS-based size measurements of aminated and PEGylated particles are shown in Table 1. As expected, the aminated particles treated with mPEG-Amine aggregated after centrifugation and resuspension in PBS. However, the particles treated with mPEG-SMB and NHS-PEG-MAL were both stable in PBS.

Table 1: Results of DLS size measurements

Silane	PEG[a]	Size after PEGylation (nm),		
		Measured in MeOH	**Measured in PBS**	**After two days in PBS**
APTES only	None	220 ± 88		
	Amine	varies, 615 -1280	Aggregated	Aggregated
	SMB	360 ± 127	271 ± 84	260 ± 70
	NPM	240 ± 95	396 ±126	371 ± 140
APTES and BTEOSE	None	235 ± 100		
	Amine	varies, 255 - 5000	Aggregated	Aggregated
	SMB	300 ± 151	314 ± 165	520 ± 200
	NPM	255 ± 100	Peaks at 190, 700, 1280 (aggregation)	326 ± 117
APTES and THPMP	None	235 ± 100		
	Amine	varies, 91 - 955	Aggregated	Aggregated
	SMB	490 and 2130	295 - 500	360 ± 200
	NPM	295 ± 126	295 ± 139	295 ± 200

[a] "Amine" refers to mPEG-Amine, "SMB" refers to mPEG-SMB, "NPM" refers to "NHS-PEG-MAL"

Particle stability was also assessed visually, as shown in Figure 10. These particles were PEGylated in methanol, washed, and re-suspended in PBS. The particles treated with mPEG-Amine could not be re-suspended, as they had formed a large aggregate at the bottom of the tube. After two days in solution, some of the particles pegylated with mPEG-SMB and NHS-PEG-MAL had settled but immediately re-dispersed after gentle flicking.
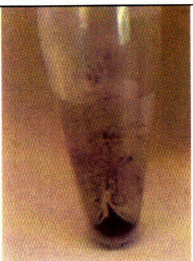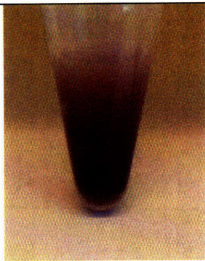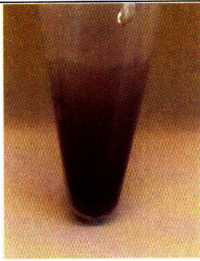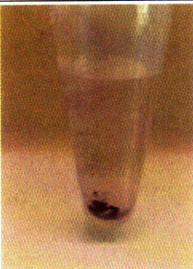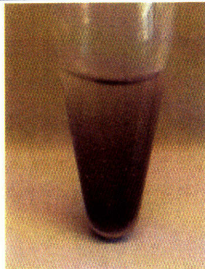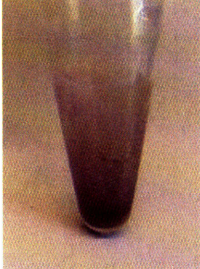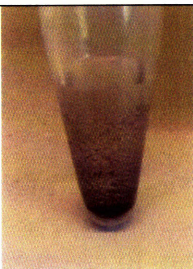
Silane	mPEG-Amine	mPEG-SMB	NHS-PEG-MAL
APTES only			
APTES & BTEOSE			
APTES & THPMP			

Figure 10: Stability of PEGylated particles after two days in PBS and gentle flicking, post amination with (a) APTES, (b) APTES and BTEOSE, and (c) APTES and THPMP.

Previous studies had demonstrated a subtle stabilizing effect of BTEOSE for 126 nm silica particles [43], but the mechanism is largely unknown and additional stabilization did not seem to occur with these particles. In fact the opposite phenomenon appears to be true, as the APTES and BTEOSE particles show more aggregation in PBS (Figure 10).

The behavior of functionalized nanoparticles can be better understood when modeled as a colloid dispersion. As previously mentioned, approximate sedimentation rates were observed to infer particle stability. Stokes Law (Eq. 1) describes the

sedimentation rate of an uncharged particle of density ρ_2 and radius a in a liquid of density ρ and viscosity η:

$$\frac{dx}{dt} = \frac{2a^2 \cdot (\rho_2 - \rho) \cdot g}{9\eta}$$

(Eq. 1)

For an uncharged silicon particle ($\rho_2 = 2.33$ g/mL) with a 100 nm radius, it should take almost 16 days to sediment from the top of an Eppendorf tube (4 cm length). In toluene and methanol, the sedimentation times are 9.9 and 8.1 days, respectively. This is consistent with our observations.

While Stokes' Law provides a good estimate for uncharged particles being acted upon by gravity, Brownian motion must also be considered. Brownian motion causes particles in colloidal solutions to interact. If they get sufficiently close to each other, the van der Waals attractive force could cause them to aggregate and flocculate. The tendency to flocculate is also affected by the electrolyte concentration of the solution. At zero or low electrolyte concentrations, the potential energy of interaction is large compared to the thermal energy of the particles, so the colloidal solution should be stable. At higher electrolyte concentrations, the energy barrier to flocculation is lower. The electrolyte concentration explains why the particles remain in solution longer in methanol and water than in PBS.

The potential energy of interaction is also dependent on the surface potential of the particles. High surface potentials increase the potential energy of interaction, thereby preventing flocculation. Since, the Zeta potential measurements indicate that the aminated particles are highly charged, both the electrolyte concentration and surface potential must be considered when estimating colloid stability [51]. This phenomenon is

evident when the particles are resuspended in solutions with high pHs that neutralize the amines on the particle surface; the particles fall out of solution faster and have a tendency to aggregate.

Overall, while the surface charge of the APTES & BTEOSE treated particles is the highest, the fluorescamine measurements do not indicate a significant difference between the degree of amination among three silane treatments. Amination with APTES alone appears to be sufficient.

4.3 Cytotoxicity of unmodified particles

The cytotoxicity of unmodified silicon particles was determined using a calcein assay. Initially, an MTT assay was used but was later abandoned because of its reported incompatibility with silicon microparticles due to the spontaneous and simultaneous reduction of MTT and oxidation of the Si particle surface [52]. Another obstacle was maintaining the stability of the unmodified particles in the serum solution. To prevent sedimentation, the segment of the protocol where particles were incubated with cells was changed from 24-hours to 3-hours, and the plate was shaken very gently. Three hours was not long enough to see measure toxicity by the caffeine control. However, the unmodified particles had a TC50 of 0.3354 mg/mL, which is the concentration required to produce toxic effects in 50% of the cells (Table 2). In comparison, caffeine's TC50 is 1.18 mg/mL and acetaminophen's TC50 is 3.17 mg/mL. This experiment could not be repeated due to time constraints.

Table 2: Cytotoxicity of (a) caffeine (control) and (b) bare silicon nanoparticles, as measured by a calcein assay.
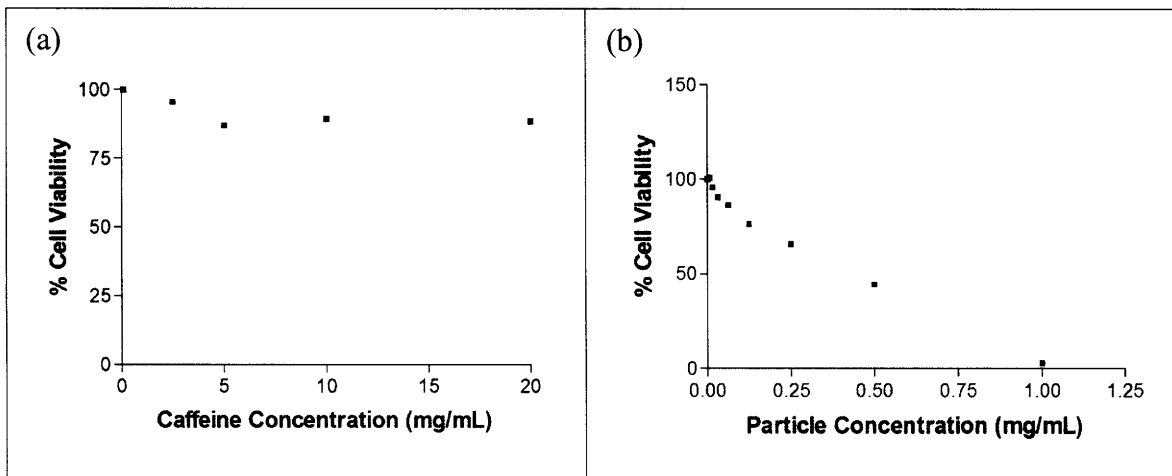
5 Conclusion and Future Work

In this thesis, I have described a reproducible method for creating PEG-coated ball-milled silicon particles. The particles have a mean diameter around 300 nm and can be aminated using APTES, or a combination of APTES with BTEOSE or THPMP. Further modification can be performed using PEG to form stable colloid solutions, as verified by DLS size measurements and visualization of sedimentation.

The next steps of this project are to determine particle cytotoxicity after pegylation, measure particle circulation times in mice, demonstrate hyperpolarization, and image functionalized particles *in vivo*. Once the biocompatibility and hyperpolarizability are confirmed, these particles have numerous very promising *in vivo* applications. The most direct application is for early tumor detection through passive targeting, which can provide doctors with information on the progress of the disease and lead to markedly improved patient outcomes. Finally, these stable, hyperpolarized nanoparticles can also be used to label and track stem cells in order to elucidate the mechanisms behind stem cell trafficking and differentiation.

6 References

[1] D. Simberg, T. Duza, J. H. Park, M. Essler, J. Pilch, L. Zhang, A. M. Derfus, M. Yang, R. M. Hoffman, S. Bhatia, M. J. Sailor and E. Ruoslahti, "Biomimetic amplification of nanoparticle homing to tumors," *Proc. Natl. Acad. Sci. U. S. A.,* vol. 104, pp. 932-936, Jan 16. 2007.

[2] D. L. Thorek, A. K. Chen, J. Czupryna and A. Tsourkas, "Superparamagnetic iron oxide nanoparticle probes for molecular imaging," *Ann. Biomed. Eng.,* vol. 34, pp. 23-38, Jan. 2006.

[3] G. Staatz, C. C. Nolte-Ernsting, G. B. Adam, S. Grosskortenhaus, B. Misselwitz, A. Bucker and R. W. Gunther, "Interstitial T1-weighted MR lymphography: lipophilic perfluorinated gadolinium chelates in pigs," *Radiology,* vol. 220, pp. 129-134, Jul. 2001.

[4] J. H. Ardenkjaer-Larsen, B. Fridlund, A. Gram, G. Hansson, L. Hansson, M. H. Lerche, R. Servin, M. Thaning and K. Golman, "Increase in signal-to-noise ratio of > 10,000 times in liquid-state NMR," *Proc. Natl. Acad. Sci. U. S. A.,* vol. 100, pp. 10158-10163, Sep 2. 2003.

[5] R. Jugdaohsingh, S. H. Anderson, K. L. Tucker, H. Elliott, D. P. Kiel, R. P. Thompson and J. J. Powell, "Dietary silicon intake and absorption," *Am. J. Clin. Nutr.,* vol. 75, pp. 887-893, May. 2002.

[6] Westbrook, C., Roth, C. K., & Talbot, J., *MRI in Practice.* Oxford: Blackwell Science Ltd., 2005,

[7] Anonymous "Contrast Agents," vol. 2008, 2008.

[8] J. Kurtkoti, T. Snow and B. Hiremagalur, "Gadolinium and nephrogenic systemic fibrosis: association or causation," *Nephrology (Carlton),* vol. 13, pp. 235-241, Jun. 2008.

[9] R. Guzman, N. Uchida, T. M. Bliss, D. He, K. K. Christopherson, D. Stellwagen, A. Capela, J. Greve, R. C. Malenka, M. E. Moseley, T. D. Palmer and G. K. Steinberg, "Long-term monitoring of transplanted human neural stem cells in developmental and pathological contexts with MRI," *Proc. Natl. Acad. Sci. U. S. A.,* vol. 104, pp. 10211-10216, Jun 12. 2007.

[10] R. Guzman, N. Uchida, T. M. Bliss, D. He, K. K. Christopherson, D. Stellwagen, A. Capela, J. Greve, R. C. Malenka, M. E. Moseley, T. D. Palmer and G. K. Steinberg, "Long-term monitoring of transplanted human neural stem cells in developmental and pathological contexts with MRI," *Proc. Natl. Acad. Sci. U. S. A.,* vol. 104, pp. 10211-10216, Jun 12. 2007.

[11] M. J. Pittet, J. Grimm, C. R. Berger, T. Tamura, G. Wojtkiewicz, M. Nahrendorf, P. Romero, F. K. Swirski and R. Weissleder, "In vivo imaging of T cell delivery to tumors after adoptive transfer therapy," *Proc. Natl. Acad. Sci. U. S. A.,* vol. 104, pp. 12457-12461, Jul 24. 2007.

[12] B. Chertok, B. A. Moffat, A. E. David, F. Yu, C. Bergemann, B. D. Ross and V. C. Yang, "Iron oxide nanoparticles as a drug delivery vehicle for MRI monitored magnetic targeting of brain tumors," *Biomaterials,* vol. 29, pp. 487-496, Feb. 2008.

[13] W. J. Rogers, C. H. Meyer and C. M. Kramer, "Technology insight: in vivo cell tracking by use of MRI," *Nat. Clin. Pract. Cardiovasc. Med.,* vol. 3, pp. 554-562, Oct. 2006.

[14] T. Maly, G. T. Debelouchina, V. S. Bajaj, K. N. Hu, C. G. Joo, M. L. Mak-Jurkauskas, J. R. Sirigiri, P. C. van der Wel, J. Herzfeld, R. J. Temkin and R. G. Griffin, "Dynamic nuclear polarization at high magnetic fields," *J. Chem. Phys.,* vol. 128, pp. 052211, Feb 7. 2008.

[15] J. C. Woods, C. K. Choong, D. A. Yablonskiy, J. Bentley, J. Wong, J. A. Pierce, J. D. Cooper, P. T. Macklem, M. S. Conradi and J. C. Hogg, "Hyperpolarized 3He diffusion MRI and histology in pulmonary emphysema," *Magn. Reson. Med.,* vol. 56, pp. 1293-1300, Dec. 2006.

[16] A. Kimura, T. Wakayama, M. Narazaki, Y. Kawata, T. Ueyama and H. Fujiwara, "Improvement of T1 determination of hyperpolarized 129Xe in mouse brain under controlled-flow," *Magn. Reson. Med. Sci.,* vol. 3, pp. 199-205, 2004.

[17] K. Golman, J. H. Ardenkjaer-Larsen, J. S. Petersson, S. Mansson and I. Leunbach, "Molecular imaging with endogenous substances," *Proc. Natl. Acad. Sci. U. S. A.,* vol. 100, pp. 10435-10439, Sep 2. 2003.

[18] C. H. Cunningham, A. P. Chen, M. Lustig, J. Lupo, D. Xu, J. Kurhanewicz, R. E. Hurd, J. M. Pauly, S. J. Nelson and D. B. Vigneron, "Pulse sequence for dynamic volumetric imaging of hyperpolarized metabolic products," *J. Magn. Reson.,* Mar 23. 2008.

[19] Ladd, T.D., Maryenko, D., Yamamoto, Y., Abe, E., and K.M. Ito, "Coherence time of decoupled nuclear spins in silicon," *Physical Reviews B,* vol. 71, pp. 014401, 2005.

[20] H. Maeda, "The enhanced permeability and retention (EPR) effect in tumor vasculature: the key role of tumor-selective macromolecular drug targeting," *Adv. Enzyme Regul.,* vol. 41, pp. 189-207, 2001.

[21] C. Heyn, J. A. Ronald, S. S. Ramadan, J. A. Snir, A. M. Barry, L. T. MacKenzie, D. J. Mikulis, D. Palmieri, J. L. Bronder, P. S. Steeg, T. Yoneda, I. C. MacDonald, A. F. Chambers, B. K. Rutt and P. J. Foster, "In vivo MRI of cancer cell fate at the single-cell level in a mouse model of breast cancer metastasis to the brain," *Magn. Reson. Med.,* vol. 56, pp. 1001-1010, Nov. 2006.

[22] L. T. Canham, "Nanoscale semiconducting silicon as a nutritional food additive," *Nanotechnology,* pp. 185704, 2007.

[23] E. Bisse, T. Epting, A. Beil, G. Lindinger, H. Lang and H. Wieland, "Reference values for serum silicon in adults," *Anal. Biochem.,* vol. 337, pp. 130-135, Feb 1. 2005.

[24] A. E. Dementyev, D. G. Cory and C. Ramanathan, "Dynamic Nuclear Polarization in Silicon Microparticles," *Physical Review Letters,* vol. 100, pp. 127601, 2008.

[25] S. Nie, Y. Xing, G. J. Kim and J. W. Simons, "Nanotechnology applications in cancer," *Annu. Rev. Biomed. Eng.,* vol. 9, pp. 257-288, 2007.

[26] R. Etzioni, N. Urban, S. Ramsey, M. McIntosh, S. Schwartz, B. Reid, J. Radich, G. Anderson and L. Hartwell, "The case for early detection," *Nat. Rev. Cancer.,* vol. 3, pp. 243-252, Apr. 2003.

[27] J. R. Dorvee, M. J. Sailor and G. M. Miskelly, "Digital microfluidics and delivery of molecular payloads with magnetic porous silicon chaperones," *Dalton Trans.,* vol. (6), pp. 721-730, Feb 14. 2008.

[28] L. R. Hirsch, R. J. Stafford, J. A. Bankson, S. R. Sershen, B. Rivera, R. E. Price, J. D. Hazle, N. J. Halas and J. L. West, "Nanoshell-mediated near-infrared thermal therapy of tumors under magnetic resonance guidance," *Proc. Natl. Acad. Sci. U. S. A.,* vol. 100, pp. 13549-13554, Nov 11. 2003.

[29] Y. J. Jun, J. I. Kim, M. J. Jun and Y. S. Sohn, "Selective tumor targeting by enhanced permeability and retention effect. Synthesis and antitumor activity of polyphosphazene-platinum (II) conjugates," *J. Inorg. Biochem.,* vol. 99, pp. 1593-1601, Aug. 2005.

[30] K. Cho, X. Wang, S. Nie, Z. G. Chen and D. M. Shin, "Therapeutic nanoparticles for drug delivery in cancer," *Clin. Cancer Res.,* vol. 14, pp. 1310-1316, Mar 1. 2008.

[31] E. Ruoslahti and M. D. Pierschbacher, "New perspectives in cell adhesion: RGD and integrins," *Science,* vol. 238, pp. 491-497, Oct 23. 1987.

[32] P. K. Dubey, V. Mishra, S. Jain, S. Mahor and S. P. Vyas, "Liposomes modified with cyclic RGD peptide for tumor targeting," *J. Drug Target.,* vol. 12, pp. 257-264, Jun. 2004.

[33] T. J. Harris, G. Von Maltzahn and S. N. Bhatia, "Multifunctional nanoparticles for cancer therapy," in *Nanotechnology for Cancer Therapy* M. M. Amiji, Ed. CRC, 2006, pp. 59-75.

[34] W. Jiang, B. Y. S. Kim, J. T. Rutka and W. C. W. Chan, "Nanoparticle-mediated cellular response is size-dependent," *Nature Nanotechnology,* vol. 3, pp. 145-150, 2008.

[35] B. D. Chithrani, A. A. Ghazani and W. C. Chan, "Determining the size and shape dependence of gold nanoparticle uptake into mammalian cells," *Nano Lett.,* vol. 6, pp. 662-668, Apr. 2006.

[36] S. M. Moghimi, A. C. Hunter and J. C. Murray, "Long-circulating and target-specific nanoparticles: theory to practice," *Pharmacol. Rev.,* vol. 53, pp. 283-318, Jun. 2001.

[37] R. A. Freitas, *Nanomedicine: Biocompatibility.* , vol. IIA, Georgetown, TX: Landes Bioscience, 2003,

[38] S. K. Hobbs, W. L. Monsky, F. Yuan, W. G. Roberts, L. Griffith, V. P. Torchilin and R. K. Jain, "Regulation of transport pathways in tumor vessels: role of tumor type and microenvironment," *Proc. Natl. Acad. Sci. U. S. A.,* vol. 95, pp. 4607-4612, Apr 14. 1998.

[39] R. K. Jain, "Transport of molecules in the tumor interstitium: a review," *Cancer Res.,* vol. 47, pp. 3039-3051, Jun 15. 1987.

[40] M. A. Dobrovolskaia and S. E. McNeil, "Immunological properties of engineered nanomaterials," *Nature Biotechnology,* vol. 2, pp. 469-478, 2007.

[41] J. M. Harris and R. B. Chess, "Effect of pegylation on pharmaceuticals," *Nat. Rev. Drug Discov.,* vol. 2, pp. 214-221, Mar. 2003.

[42] N. R. Jana, C. Earhart and J. Y. Ying, "Synthesis of Water-Soluble and Functionalized Nanoparticles by Silica Coating," *Chem. Mater.,* vol. 19, pp. 5074-5082, 2007.

[43] Z. Zhang, A. E. Berns, S. Willbold and J. Buitenhuis, "Synthesis of poly(ethylene glycol) (PEG)-grafted colloidal silica particles with improved stability in aqueous solvents," *J. Colloid Interface Sci.,* vol. 310, pp. 446-455, Jun 15. 2007.

[44] I. Biotium, "Calcein AM Cell Viability Assay Kit,"

[45] W. Posthumus, P. C. Magusin, J. C. Brokken-Zijp, A. H. Tinnemans and R. van der Linde, "Surface modification of oxidic nanoparticles using 3-methacryloxypropyltrimethoxysilane," *J. Colloid Interface Sci.,* vol. 269, pp. 109-116, Jan 1. 2004.

[46] E. R. Pohl and A. Chaves, "Sterically hindered silanes for waterborne systems: A model study of silane hydrolysis," in *Silanes and Other Coupling Agents* , vol. 3, K. L. Mittal, Ed. Ultrecht: VSP, 2004, pp. 3-10.

[47] L. Chu, M. W. Daniels and L. F. Francis, "Use of (Glycidoxypropyl)trimethoxysilane as a Binder in Colloidal Silica Coatings," *Chem. Mater.,* vol. 9, pp. 2577-2582, 1997.

[48] B. G. Tilset, F. Lapique, A. Bjorgum and C. Simensen, "Amino- and bis-silane pre-treatments for adhesive bonding of aluminum," in *Silanes and Other Coupling Agents* , vol. 3, K. L. Mittal, Ed. Utrecht: VSP, 2004, pp. 51-68.

[49] J. A. Howarter and J. P. Youngblood, "Optimization of silica silanization by 3-aminopropyltriethoxysilane," *Langmuir,* vol. 22, pp. 11142-11147, Dec 19. 2006.

[50] H. Xu, F. Yan, E. E. Monson and R. Kopelman, "Room-temperature preparation and characterization of poly (ethylene glycol)-coated silica nanoparticles for biomedical applications," *J. Biomed. Mater. Res. A.,* vol. 66, pp. 870-879, Sep 15. 2003.

[51] D. J. Shaw, *Introduction to Colloid and Surface Chemistry.* London: The Butterworth Group, 1970, pp. 236.

[52] T. Laaksonen, H. Santos, H. Vihola, J. Salonen, J. Riikonen, T. Heikkila, L. Peltonen, N. Kumar, D. Y. Murzin, V. P. Lehto and J. Hirvonen, "Failure of MTT as a toxicity testing agent for mesoporous silicon microparticles," *Chem. Res. Toxicol.,* vol. 20, pp. 1913-1918, Dec. 2007.

[53] R. Gref, Y. Minamitake, M.T. Peracchia, V. Trubetskoy, V. Torchilin, and R. Langer, "Biodegradable Long-Circulating Polymeric Nanospheres," *Science,* vol. 263, pp. 1600-1603, Mar. 1994.